Article

Not peer-reviewed version

Bimodal Regime Structure in Galactic Rotation Curves: Evidence for Distinct Dynamical States and a Field-Based Interpretation of the Dark Matter Effect

Ukshin Q. Rexhepi *

Posted Date: 9 April 2026

doi: 10.20944/preprints202604.0640.v1

Keywords: galactic rotation curves; dark matter; radial acceleration relation; SPARC; galaxy dynamics; alternative gravity; astrophysics; UQSH; universal quantum foam hypothesis

 doi:10.20944/preprints202604.0640.v1

Article

Bimodal Regime Structure in Galactic Rotation Curves: Evidence for Distinct Dynamical States and a Field-Based Interpretation of the Dark Matter Effect

Ukshin Q. Rexhepi

Independent Researcher, Tübingen, Germany; ukshin.rexhepi@gmail.com

Abstract

This work analyses 164 galactic rotation curves from the SPARC database and develops a field-based interpretation of the dark matter effect within the framework of the Universal Quantum Foam Hypothesis (UQSH). The empirical excess term $C(r) = v_{\mathrm{obs}}^2(r) - v_{\mathrm{bar}}^2(r)$ reveals, after normalisation, a consistent structure of preferred dynamical regimes. Global fits identify two dominant states: a peak regime with scale parameter $q \approx 0.5$–1.0, encompassing mainly low-surface-brightness galaxies and dwarf galaxies, and a diffuse regime with $q \approx 3.0$, dominated by more massive spiral galaxies. Individual fits yield a distribution of roughly 62% peak systems, 26% diffuse systems, and 12% in the transition zone. An analysis of the dynamic factor $D = g_{\mathrm{obs}}/g_{\mathrm{bar}}$ as a function of the maximum rotation curve radius reveals a statistically significant negative correlation ($r = -0.31$, $p = 0.0001$). Beyond approximately 50–80 kpc, D converges systematically toward 1. This empirical instability boundary marks the spatial range within which coherent field organisation produces measurable amplification. In the UQSH, light is interpreted as a spherically propagating tension front that follows the accumulated field geometry. In this picture, the convergence κ does not measure the instantaneous mass density, but the projected field curvature. A UQSH model of the Bullet Cluster reproduces the characteristic order of magnitude of the offsets between gas centres and κ-peaks of 219 kpc and 228 kpc without requiring an additional non-baryonic matter component. In the UQSH, the dark matter effect is not a sign of missing particles but an intrinsic property of the field medium. Baryonic structures are stable field configurations that spatially pre-stress the field medium. Through continuous radiation they excite the field and generate persistent deformations that do not fully relax. The nonlinear superposition of these three sources — bound baryonic mass, continuous radiation, and the accumulated field pre-stress — produces a large-scale field tension that appears observationally as the dark matter effect. On galactic scales, the empirical instability boundary at approximately 50–80 kpc sets a natural spatial limit on this field tension. In galaxy clusters, the individual contributions of many saturated structures superpose into a collective field tension that systematically raises the lensing signal above the baryonic expectation. The universal fits show high internal consistency within each regime, with mean squared errors of MSE ≈ 0.016 in the peak regime and MSE ≈ 0.06–0.13 in the diffuse regime. This universality stands in contrast to the expectation from continuous halo models and supports the field-based interpretation of preferred dynamical states.

Keywords: galactic rotation curves; dark matter; radial acceleration relation; SPARC; galaxy dynamics; alternative gravity; astrophysics; UQSH; universal quantum foam hypothesis

1. Introduction

1.1. Background

Galactic rotation curves, gravitational lensing, and large-scale structure formation all point to the same problem: the gravitational effect of visible matter is not sufficient to explain the observed

 doi:10.20944/preprints202604.0640.v1

dynamics of astrophysical systems. For decades, dark matter has served as the explanation — a non-luminous matter component that acts gravitationally but has so far not been directly detected.

Despite substantial experimental effort, the particle nature of dark matter has remained unconfirmed. This has motivated the search for alternatives: approaches that do not postulate a new substance, but instead interpret the origin of the observed effects differently.

The present work takes such a path. The starting point is a continuous field medium in which observable matter corresponds to stable, coupling-capable organisational states. Alongside these exist non-coupling structures that contribute to gravitational dynamics without being directly visible. Within this framework, dark matter does not appear as a particle but as an effect of field organisation itself.

1.2. Intuitive Reading of the Excess Dynamics

The empirical excess term

$$C(r) = v_{\mathrm{obs}}^2(r) - v_{\mathrm{bar}}^2(r) \tag{1}$$

describes how strongly the underlying field medium responds to the existing matter structure beyond the baryonic contribution. It is directly accessible from observational data and requires no model assumptions about the nature of this response.

The analysis shows that this excess response is not distributed arbitrarily. Instead, two preferred forms emerge: a localised response with a pronounced maximum at a particular radial range — the *peak regime* — and a broadly distributed response with no characteristic maximum extending over large radii — the *diffuse regime*. Intuitively, these correspond to two different ways the field responds to matter: either concentrated at a specific location, or spread evenly across the system.

1.3. Motivation and Objectives

This work pursues two goals. First, the effective excess term $C(r)$ is systematically extracted and characterised from a large sample of rotation curves from the SPARC database. Second, the work investigates whether the observed structure of this term is consistent with a field-based interpretation within the Universal Quantum Foam Hypothesis (UQSH).

1.4. Structure of the Paper

The paper is structured as follows:

Section 2 gives an overview of the observational motivation for dark matter and introduces the basic field-based interpretation.

Section 3 describes the data and the methodology used to extract the excess term.

Section 4 presents the central empirical results, in particular the identification of preferred dynamical regimes.

Section 5 develops the empirical foundation of structure-dependent field dynamics. Based on the SPARC sample, two saturation levels and an empirical instability boundary at approximately 50–80 kpc are identified.

Section 6 develops the physical interpretation within the UQSH, including the conceptual framing of the dark matter effect as an expression of persistent field organisation, along with testable predictions.

Section 7 formalises gravitational lensing within the UQSH framework. Light is interpreted as a tension front following the accumulated field geometry. The κ definition is derived from the field structure and quantitatively tested against the Bullet Cluster.

Section 8 describes the accumulation of field tension in galaxy clusters and derives predictions for merging clusters such as El Gordo and MACS J0717.

Section 9 presents the dark matter effect as a direct consequence of the described field processes and identifies three structurally distinct sources of the additional gravitational effect.

 doi:10.20944/preprints202604.0640.v1

Section 10 compares the results with standard models and discusses the significance of the observed regime structure.

Section 11 presents the results on the regime-dependent improvement of the velocity definition in the baryonic Tully-Fisher relation.

Section 12 discusses the main results, addresses open questions, gives an outlook on future work, and summarises the central findings.

2. Observational Motivation

2.1. Galactic Rotation Curves

A central motivation for dark matter comes from galactic rotation curves. For a particle at distance r from the centre, classical mechanics predicts:

$$v(r) \sim \sqrt{\frac{GM(r)}{r}}, \tag{2}$$

which for a finite mass distribution should lead to a declining velocity with increasing radius.

Observations, however, show that rotation curves in the outer regions of galaxies typically remain flat [6]:

$$v(r) \approx \text{constant}. \tag{3}$$

This implies that the effective enclosed mass $M(r)$ continues to grow with radius. Additional evidence comes from gravitational lensing and the dynamics of galaxy clusters [10], which also point to gravitational contributions that are not electromagnetically visible.

2.2. Radial Acceleration Relation

A particularly instructive empirical finding is the Radial Acceleration Relation (RAR) [1]. It describes the observed relationship between the radial acceleration expected from the baryonic matter distribution and the dynamical acceleration actually derived from rotation curves. This tight coupling was first approached theoretically by [7] through a modification of Newtonian dynamics.

Remarkably, the additional gravitational effect is not distributed independently of visible matter — it follows it in a strikingly systematic way. In particle-based halo models, this tight coupling is an additional structure that requires explanation. Within the field-based framework of this work, it reads naturally: the excess dynamics does not arise independently of baryonic organisation, but is structurally linked to it.

2.3. Field-Based Interpretation

This work rests on a continuous field medium whose organisation exhibits different stability and coupling states. A distinction is made between coupling-capable field structures, which appear as visible matter, and non-coupling field structures, which are not directly observable. Both types contribute to gravitational dynamics. Non-coupling structures are not physically inert — they are simply not directly visible in the relevant observational regime. Observable matter thus represents only a part of the total field organisation.

2.4. Effective Density Model

To describe the total gravitational effect, an effective mass density is introduced:

$$\rho_{\text{eff}} = \rho_{\text{visible}} + \rho_{\text{sub}}, \tag{4}$$

where ρ_{sub} describes the contributions of non-coupling field structures. The gravitational potential equation then becomes:

$$\nabla^2 \Phi = 4\pi G \rho_{\text{eff}}. \tag{5}$$

 doi:10.20944/preprints202604.0640.v1

For extended distributions of ρ_{sub}, the effective mass can continue to grow with radius, giving rise to flat rotation curves. No additional particle component is needed for this.

3. Data and Methodology

3.1. The SPARC Database

The analysis is based on rotation curves from the SPARC database (Spitzer Photometry and Accurate Rotation Curves) [2]. SPARC contains high-quality rotation curves for 175 galaxies with HI and/or Hα velocity measurements, photometric data at 3.6 μm (Spitzer), mass models for gas, disc, and bulge, radii up to 20–40 kpc, and a mass range of 10^8 to 10^{11} $M_\odot$. Of the 175 available galaxies, 164 systems were included in the analysis, after excluding systems with incomplete data or insufficient radial coverage.

3.2. Extraction of the Excess Term

For each galaxy, the effective excess term was determined directly from the observational data. The starting point is:

$$v_{\mathrm{obs}}^2(r) = v_{\mathrm{bar}}^2(r) + C(r), \tag{6}$$

where $v_{\mathrm{obs}}(r)$ is the observed rotation velocity and $v_{\mathrm{bar}}(r)$ is the baryonic contribution, given by:

$$v_{\mathrm{bar}}^2(r) = v_{\mathrm{gas}}^2(r) + a\, v_{\mathrm{disk}}^2(r) + b\, v_{\mathrm{bulge}}^2(r), \tag{7}$$

where a and b are scaling parameters. In the standard analysis, $b = 1$ was fixed and a was varied systematically over the range $a \in [0.2, 1.0]$. A reference value of $a = 0.5$ was used, in line with the mass-to-light ratio established for SPARC galaxies at 3.6 μm [2]. The stability of the results under variations of a is discussed in Section 4.4. The excess term then follows directly as:

$$C(r) = v_{\mathrm{obs}}^2(r) - v_{\mathrm{bar}}^2(r). \tag{8}$$

Negative values of $C(r)$ were treated as non-physical and set to zero. This typically affects the outermost radial range, where measurement uncertainties dominate.

3.3. Normalisation and Shape Function

To make different galaxies comparable, a normalisation was introduced:

$$x = \frac{r}{R}, \qquad F(x) = \frac{C(r)}{C_{\mathrm{max}}}, \tag{9}$$

where C_{max} is the maximum of $C(r)$ and R is the radial position of that maximum. The normalised function $F(x)$ describes only the shape of the excess term, independently of amplitude and physical scaling.

3.4. Parametric Fit

A parametric ansatz was chosen for the normalised shape function:

$$F(x) = \frac{x^p\, e^{-x/q}}{\max_{y>0}\left(y^p e^{-y/q}\right)}, \tag{10}$$

where p is the shape exponent and q the scale parameter. The normalisation by the maximum ensures $\max F(x) = 1$. The parameters p and q were determined individually for each galaxy by minimising the squared deviation:

$$\mathrm{MSE} = \frac{1}{N}\sum_{i=1}^{N}[F(x_i) - F_{\mathrm{fit}}(x_i)]^2. \tag{11}$$

 doi:10.20944/preprints202604.0640.v1

In addition, global fits over subsamples were performed to test whether groups of galaxies share a common shape function.

3.5. Regime Classification

Galaxies were classified into two main regimes based on the extracted parameters: the peak regime with $q < 1.2$ and a pronounced internal maximum of $F(x)$, and the diffuse regime with $q > 2.5$ and a monotone or broadly distributed profile. The transition zone $1.2 \leq q < 2.5$ was investigated separately.

The chosen boundaries reflect the observed clustering of parameter values and serve to clearly separate the dominant regions of parameter space. The underlying distribution is continuous but shows distinctly preferred regions.

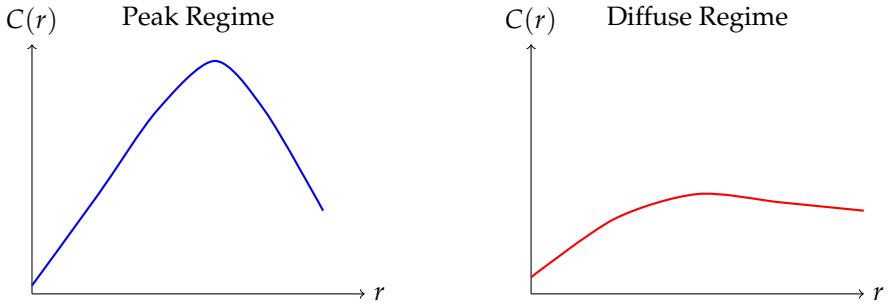

Figure 1. Schematic illustration of the two dynamical regimes of the excess term $C(r)$. In the peak regime, the additional field effect is localised with a pronounced maximum. In the diffuse regime, the field effect is broadly distributed with no characteristic peak.

4. Results

4.1. Structure of the Excess Term

The functions $C(r)$ extracted from the observational data show consistent qualitative features across different galaxies: an initial rise in the inner region, a pronounced maximum at a characteristic scale R, and a subsequent flattening or slight decline in the outer region. This structure differs clearly from classical monotone halo profiles such as NFW [5] and points to a non-trivial radial dynamics.

4.2. Bimodal Regime Structure

After normalising the excess terms according to $F(x) = C(r)/C_{\max}$ and $x = r/R$, global fits over subsamples reveal a consistent structure of preferred regimes. Table 1 summarises these results for various galaxy subsamples.

Table 1. Overview of global fits over various galaxy subsamples. Listed are the number of analysed systems (n), typical fit parameters (p, q), and the dominant regime.

Sample	n	p	q	Regime
F galaxies	15–16	1.2–1.6	0.7–1.0	peak-dominated
D galaxies	4	1.0–1.4	0.5–0.8	peak-dominated
ESO / DDO	9	0.66–0.70	∼3.0	diffuse-dominated
IC / KK	3	0.8–1.1	∼3.0	diffuse-dominated
NGC	58–63	0.62–0.93	∼3.0	diffuse-dominated
UGC / UGCA	77–79	0.66–0.78	∼3.0	diffuse-dominated
Total	164			

4.2.1. Peak Regime

The peak regime is characterised by a scale parameter $q \approx 0.5$–1.0, a shape exponent $p \approx 1.0$–1.6, a pronounced internal maximum of the normalised shape function, and a mean squared error of the global fit of MSE ≈ 0.016. In the global fits it is dominated mainly by low-surface-brightness galaxies

 doi:10.20944/preprints202604.0640.v1

(F-type) and selected dwarf galaxies. After normalisation, the profiles of these systems collapse onto a common universal curve:

$$F(x) = \frac{x^{1.22}\, e^{-x/0.45}}{\max_{y>0}\left(y^{1.22} e^{-y/0.45}\right)}. \tag{12}$$

Individual fits per galaxy reach MSE ≈ 0.003. The difference between the global and individual fit quantifies the universality: despite different amplitudes and scales, all peak systems share the same normalised profile shape.

4.2.2. Diffuse Regime

The diffuse regime is characterised by a scale parameter $q \approx 3.0$, a shape exponent $p \approx 0.6$–0.9, a monotone or broadly distributed profile with no pronounced peak, and a mean squared error of the global fit of MSE ≈ 0.06–0.13. In the global fits it is dominated mainly by the large catalogue groups NGC and UGC/UGCA, as well as IC/KK and parts of the ESO/DDO samples. The typical shape function is:

$$F(x) = \frac{x^{0.7}\, e^{-x/3.0}}{\max_{y>0}\left(y^{0.7} e^{-y/3.0}\right)}. \tag{13}$$

Individual fits per galaxy reach MSE ≈ 0.007. The higher scatter in the global fit compared to the peak regime (0.06–0.13 vs. 0.016) reflects the greater diversity of the systems included — NGC, UGC/UGCA, and ESO/DDO cover a broader range of galaxy types than the F and D samples of the peak regime.

4.3. Population of the Transition Zone

A complementary analysis based on individual fits for all 164 evaluated galaxies shows that the distribution of the scale parameter q has two preferred regions, but no strictly empty transition zone. About 62.2% of systems lie in the peak regime ($q < 1.2$), about 25.6% in the diffuse regime ($q > 2.5$), while the range $1.2 \leq q < 2.5$ contains around 12.2% of galaxies.

As Figure 2 shows, the distribution of q concentrates in two preferred regions: a peak-dominated region at small q values and a secondary concentration around $q \approx 3$. The breakdown by galaxy type in Figure 3 makes clear that this distribution is not random but systematically linked to galaxy class. Dwarf and low-surface-brightness galaxies lie predominantly in the peak regime, while large spiral galaxies show a much broader spread across peak, transition, and diffuse states.

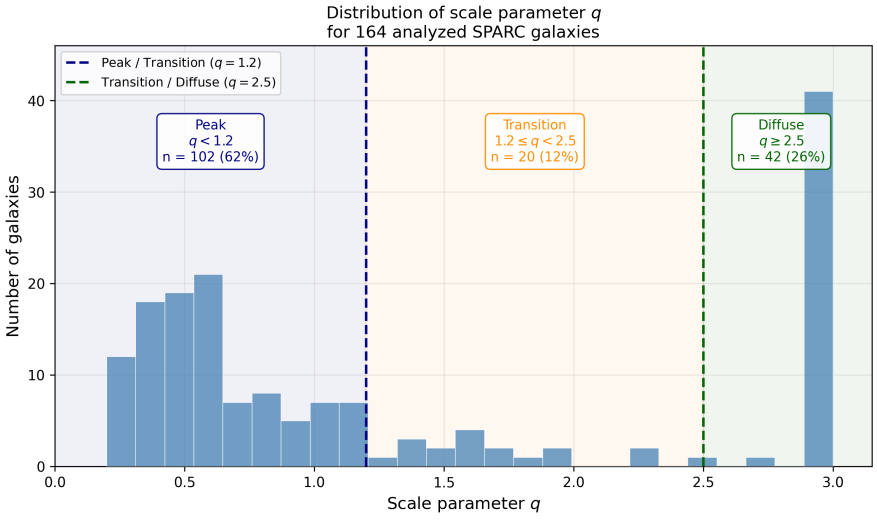

Figure 2. Distribution of the shape parameter q for all analysed SPARC galaxies. The distribution shows a bimodal structure with a dominant population at small q values (peak systems) and a secondary concentration around $q \approx 3$ (diffuse systems). The transition zone is sparsely but not emptily populated, pointing to a continuous transition between the dynamical regimes.

 doi:10.20944/preprints202604.0640.v1

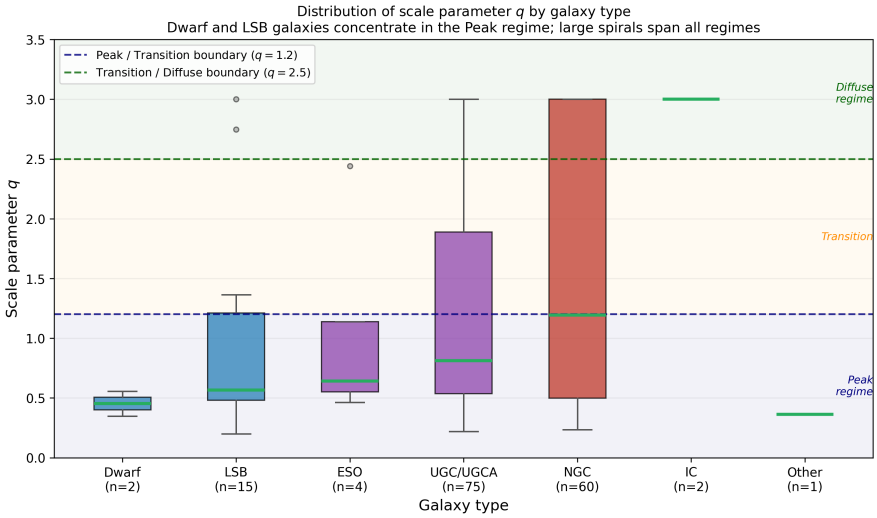

Figure 3. Distribution of the shape parameter q by galaxy type. Dwarf and low-surface-brightness galaxies show a clear concentration in the peak regime, while large spiral galaxies display a broader distribution.

The distribution is not strictly bimodal. It shows two preferred dynamical states with a sparsely populated but real transition zone. The observed regime structure is not an artefact of the chosen parametrisation — it is already visible in the normalised data themselves and remains stable under variation of the fit parameters.

Table 2. Distribution of dynamical regimes by galaxy type, based on individual fits.

Type	Peak	Transition	Diffuse
Dwarf galaxies (DDO/D)	6	1	0
ESO	3	1	0
IC	0	0	2
LSB (F)	11	2	2
NGC	30	9	21
UGC/UGCA	51	7	17
Other	1	0	0

The population of the three zones follows approximately the ratio Peak : Transition : Diffuse $\approx 31 : 6 : 13$. The peak regime dominates the sample; the transition zone is clearly more sparsely populated.

4.4. Dependence on the Baryonic Scaling Parameter

The regime structure depends systematically on the baryonic scaling parameter a, which weights the stellar disc contribution. At low values $a \lesssim 0.6$, the peak structure is stable, the separation of preferred zones in the global fits is clear, and the scatter within subsamples is small. At high values $a \gtrsim 0.8$, systems that were originally peak-dominated shift toward more diffuse behaviour, fit quality deteriorates, and parameter scatter increases. The observed excess dynamics is therefore not independent of baryonic structure, but systematically coupled to it.

4.5. Universality within the Regimes

Within each regime, the normalised profiles show a remarkable universality. In the peak regime, the profiles of various F and D galaxies collapse onto a common curve after normalisation; the scatter is typically explained by measurement uncertainties (MSE ≈ 0.016). In the diffuse regime, a consistent shape is visible across different catalogue groups, with the higher scatter (MSE ≈ 0.06–0.13) attributable to the greater diversity of the included systems. This universality stands in contrast to the expectation from individually fitted halo profiles and points to a generic property of the underlying dynamics.

 doi:10.20944/preprints202604.0640.v1

4.6. Complete Description of Rotation Curves

The complete description of the observed rotation curves is:

$$v_{\mathrm{obs}}^2(r) = v_{\mathrm{bar}}^2(r) + C_{\max}\, F\Big(\frac{r}{R}\Big), \tag{14}$$

where the shape $F(x)$ is regime-specific, and only the amplitude $C_{\max}$ and the scale R vary from galaxy to galaxy.

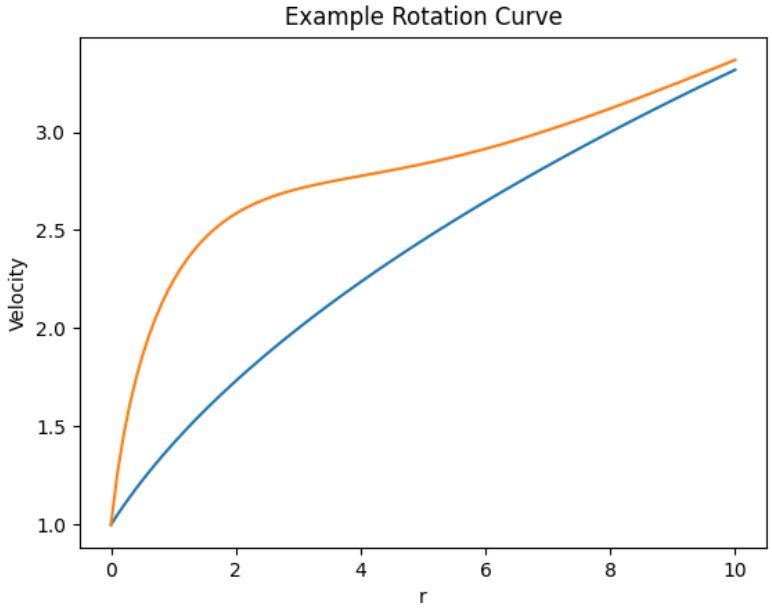

Figure 4. Schematic illustration of a rotation curve. The observed velocity is composed of the baryonic contribution and an additional field-induced dynamics. The additional dynamics corresponds to the empirical excess term $C(r)$ and typically shows a non-trivial radial structure.

Typical residuals between model and observation lie in the range $\langle \Delta v \rangle \approx 1$–$3\,\mathrm{km/s}$, which is within the typical measurement uncertainties.

4.7. Radial Acceleration Relation

The accelerations computed from the SPARC rotation curves reproduce the well-known Radial Acceleration Relation (RAR). A tight coupling between baryonic and observed dynamics is clearly visible.

Figure 10 shows the RAR colour-coded by inner structural class. Core-like, intermediate, and cuspy-like systems all lie on the same global relation. The inner profile shape does not separate the systems. This means the RAR describes a universal property of the dynamics that is independent of the specific inner mass distribution.

A simple power-law fit of the form $g_{\mathrm{add}} \propto g_{\mathrm{bar}}^{n}$ provides only an approximate description of the data. The precise functional form of the RAR is not derived in this work. It is treated as a robust phenomenological finding whose field-mechanical interpretation is developed in Section 9.6.3.

5. Field Organisation, Saturation, and Structure-Dependent Field Dynamics

The physical field of the Qu-foam takes up tension. Baryonic structures such as stars, galaxies, and clusters are not merely mass — they are active sources of continuous field excitation. The more coherent and compact a structure, the stronger and more localised the field tension it generates.

This tension does not grow without limit. Above a system-specific maximum, saturation sets in. The field can no longer absorb additional local tension and redistributes the excess outward. This

 doi:10.20944/preprints202604.0640.v1

redistribution process follows the existing field geometry and reinforces existing structures in the outer regions.

5.1. Two Saturation Levels

The analysis of the SPARC sample shows that saturation is not universal but depends on the internal structure of the system.

Compact systems in the peak regime reach their saturation locally and centrally. The relative field amplification is strong because the baryonic base is concentrated. The median dynamic factor $D = g_{\mathrm{obs}}/g_{\mathrm{bar}}$ is 2.15, at a median baryonic mass of $7.35 \times 10^9\, M_\odot$.

Large diffuse systems reach their saturation at a higher absolute field level, but the relative amplification is weaker. The median dynamic factor is 1.34, at a median baryonic mass of $3.60 \times 10^{10}\, M_\odot$ — almost five times higher. The field tension there spreads over larger spatial scales without concentrating locally.

5.2. Empirical Instability Boundary

An analysis of the median dynamic factor D_{median} as a function of the maximum rotation curve radius R_{max} yields a statistically significant negative correlation ($r = -0.31$, $p = 0.0001$).

At small radii below 20 kpc, D_{median} scatters strongly upward; values up to 8 and higher are possible. As the radius grows, D_{median} declines systematically toward 1. Beyond approximately 50–80 kpc, almost all systems lie near or below $D_{\mathrm{median}} = 2$, many already close to 1.

Beyond a spatial extent of approximately 50–80 kpc, the field can no longer build up coherent relative amplification. The field organisation disperses, the relative excess dynamics vanishes, and visible mass increasingly dominates the dynamics on its own.

This boundary is not a model assumption. It follows directly from the observational data. In the standard picture, the same behaviour is interpreted as a property of dark matter halo scaling. In the UQSH, it is a natural consequence of the limited coherence length of field-mechanical organisation.

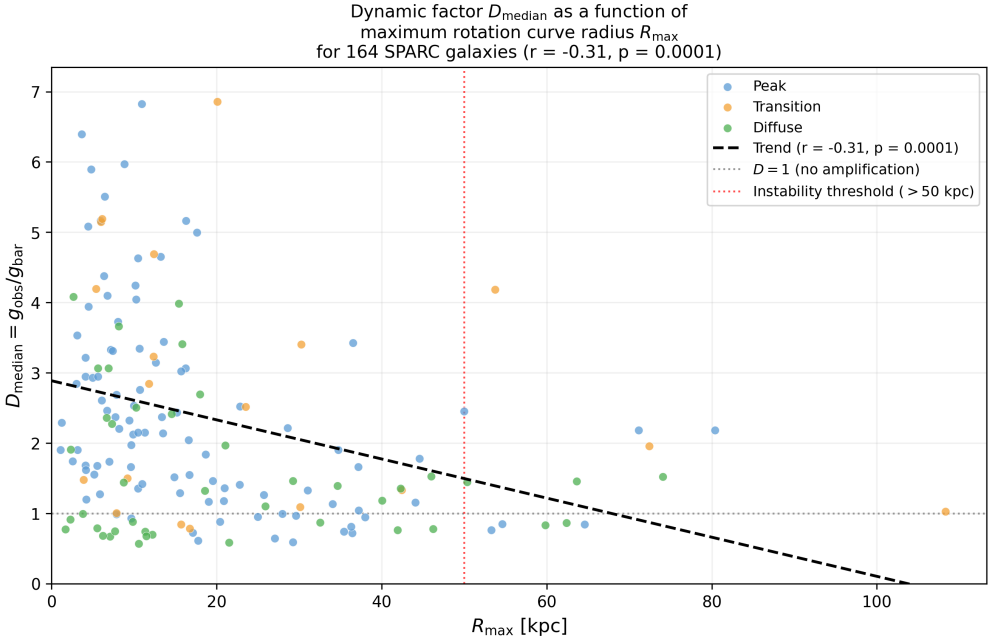

Figure 5. Dynamic factor $D_{\mathrm{median}} = g_{\mathrm{obs}}/g_{\mathrm{bar}}$ as a function of the maximum rotation curve radius R_{max} for 164 SPARC galaxies, split by dynamical regime. The dashed trend line shows a significant negative correlation ($r = -0.31$, $p = 0.0001$). Beyond approximately 50–80 kpc, D_{median} converges toward 1, indicating a structure-dependent instability boundary of coherent field organisation.

 doi:10.20944/preprints202604.0640.v1

5.3. Connection to the Dark Matter Effect

The observable dark matter effect is the measurable consequence of this structure-dependent field organisation. Flat rotation curves, enhanced gravitational lensing, and mass excess in clusters do not arise from a separate matter component, but from accumulated field tension below the instability boundary.

Above this boundary, the field loses its capacity for coherent organisation. The dynamics of large systems is increasingly determined by their visible mass — not because dark matter is absent, but because the field organisation spatially disperses and weakens.

6. Gravitational Lensing in the UQSH Framework

6.1. Light as a Tension Front

In the UQSH, light is not passive radiation following a given spacetime curvature. It is a tension front moving along the existing field configuration of the Qu-foam. Deflection occurs where the field exhibits gradients — where the accumulated field tension varies spatially.

The field itself is pre-stressed by baryonic structures. Stars and galaxies continuously generate field excitation and build up persistent field tension over their lifetimes. This tension does not fully relax but is preserved as large-scale field organisation. Light travels through this pre-stressed field and is deflected by its gradients. A direct back-reaction of light propagation on the field curvature is not measurable in the observable regime.

6.2. Consequence for Gravitational Lensing

In this framework, gravitational lensing does not measure the instantaneous local mass density, but the accumulated field tension along the line of sight. This is systematically larger than the baryonic contribution alone, because radiation-induced field excitation is persistent and does not vanish with the radiation itself.

The convergence κ, which in standard theory describes the projected mass density, is interpreted in the UQSH as projected field curvature:

$$\kappa_{\mathrm{UQSH}}(x,y) = \frac{1}{\Phi_{\mathrm{crit}}} \int \nabla^2 \phi_{\mathrm{tot}}(x,y,z)\, dz, \tag{15}$$

where ϕ_{tot} is the total field comprising baryonic and radiation-induced contributions:

$$\phi_{\mathrm{tot}} = \phi_{\mathrm{bar}} + \phi_{\mathrm{rad}}. \tag{16}$$

The deflection angle follows from the gradients of the integrated field tension:

$$\vec{\alpha}(x,y) \propto \nabla_{x,y} \int \phi_{\mathrm{tot}}(x,y,z)\, dz. \tag{17}$$

Functionally this corresponds to the classical lens equation. The ontological difference is that not mass, but the organisation of the field medium determines the deflection.

6.3. Connection to Saturation

The structure-dependent field saturation described in Section 5 directly affects lensing strength. Below the instability boundary of approximately 50–80 kpc, the field accumulates coherent tension exceeding the baryonic contribution. Above it, the field tension disperses spatially and the relative amplification decreases.

For galaxy clusters this means: many saturated structures together generate a large-scale field tension that systematically raises the lensing signal above the baryonic expectation. This is not evidence for additional matter, but a direct consequence of accumulated field organisation.

 doi:10.20944/preprints202604.0640.v1

6.4. Empirical Test: The Bullet Cluster

The Bullet Cluster provides a direct empirical test of this interpretation. If κ measures projected field tension rather than instantaneous mass density, the κ-peaks follow the coherent, structurally stable components of the system. Galaxies largely retain their field tension even under dynamic conditions, while the hot gas responds dissipatively during the collision and loses its coherent field contribution.

The measured offsets between gas centres and κ-peaks are 219 kpc and 228 kpc, with a mean of $\sim$223 kpc. The UQSH model reproduces this order of magnitude without requiring an additional non-baryonic matter component.

Caveat: A complete quantitative derivation of κ_{UQSH} from the field equation remains for future work. Equation (15) is to be understood as a conceptual working approach, not a closed dynamical derivation.

6.5. Quantitative Comparison with the Bullet Cluster

For the quantitative test, the UQSH model was applied to a Bullet-Cluster-like geometry. Two galaxy centres at $+200$ kpc and -160 kpc relative to the system barycentre generate the baryonic field structure; the gas centre lies at $+30$ kpc. The κ-map follows from the negative Laplacian of the total field, projected along the line of sight.

The model places two κ-peaks at $x = +199$ kpc and $x = -162$ kpc. Their distances to the gas centre are 169 kpc and 192 kpc, with a mean of $\sim$181 kpc.

Clowe et al. (2006) measure offsets of 219 kpc and 228 kpc, with a mean of $\sim$223 kpc [3]. The model values thus lie 15–25% below the observed values.

This discrepancy is not surprising. The galaxy positions and gas centre offset were set approximately; the field parameters σ_{gal}, σ_{gas}, and α_{gas} were not optimised. The model reproduces the characteristic spatial separation between gas centre and κ-peaks without any adjustment to the observational data.

Note on data availability: The original data from Clowe et al. (2006) were requested from the first author. No reply had been received by the time this manuscript was completed. A calibration of the model to the real Bullet Cluster geometry — with precise galaxy and gas centre positions as well as lensing convergence profiles — remains for future work. A significantly better quantitative agreement is then to be expected.

Preprints.org (www.preprints.org) | NOT PEER-REVIEWED | Posted: 9 April 2026 doi:10.20944/preprints202604.0640.v1

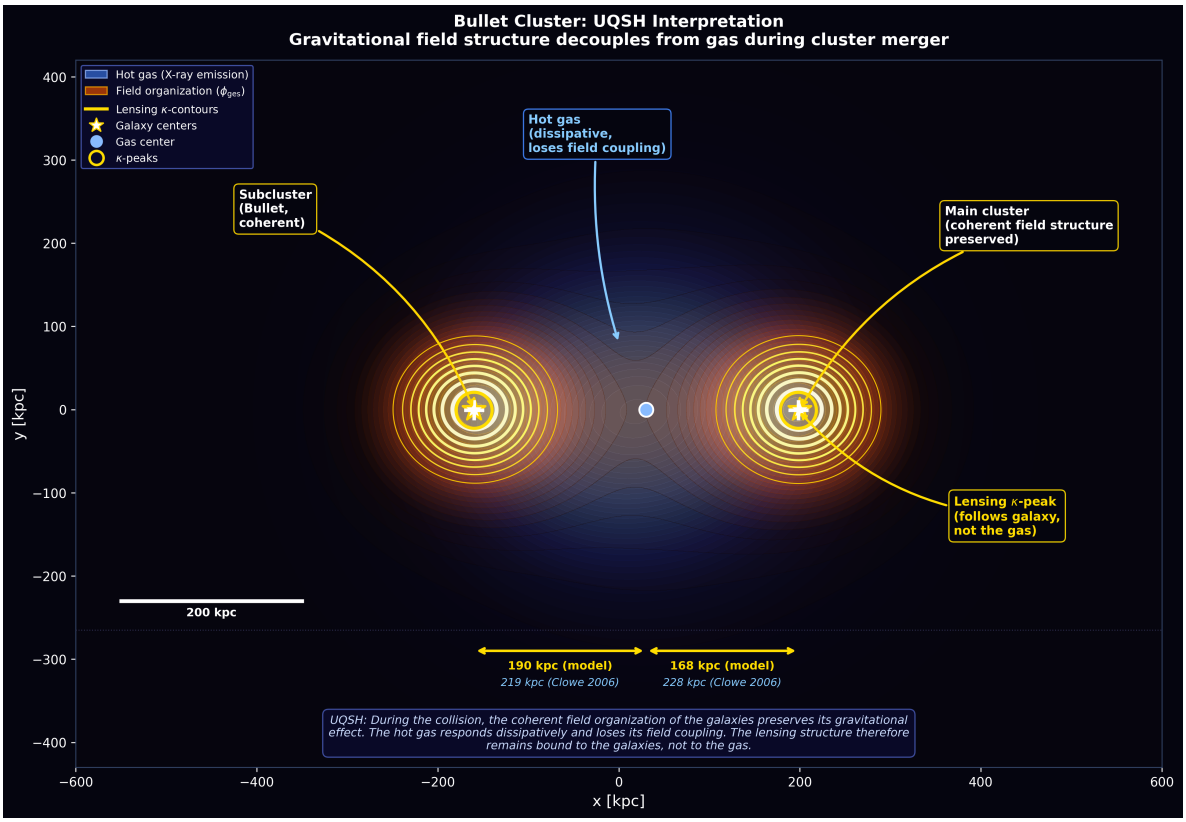

Figure 6. UQSH gravitational lensing model for a Bullet Cluster analogue. (A) Total field $\phi_{\rm tot}$ from baryonic and radiation-induced contributions. The two galaxy centres generate local field maxima; the gas centre lies between the two components. (B) UQSH κ-map as projected field curvature $\kappa \propto \int \nabla^2 \phi_{\rm tot}\, dz$. The two κ-peaks follow the galaxy centres and are spatially separated from the gas centre. (C) Deflection field $\vec{\alpha} \propto \nabla \int \phi_{\rm tot}\, dz$. Deflection is strongest near the galaxy centres. The κ-peak distances to the gas centre are 169 kpc and 192 kpc in the model, compared to 219 kpc and 228 kpc in the observation [3,12].

7. Accumulation of Field Tension in Galaxy Clusters

Individual galaxies generate local field tension that remains coherently organised below the instability boundary described in Section 5. In galaxy clusters, these individual contributions superpose. The total field is not the simple sum of the individual fields, but the result of the nonlinear superposition of persistent field organisation.

7.1. Mechanism of Accumulation

Every baryonic structure continuously generates field excitation. This excitation propagates through the field medium and leaves persistent deformations that do not fully relax. In isolated galaxies, the accumulated field tension remains confined to the system. In clusters, the field deformations of many galaxies superpose spatially and temporally.

The resulting total field tension exceeds the sum of the individual contributions, because coherent superpositions amplify the local field curvature. This effect is analogous to constructive interference in wave fields, but differs in that the superposition is persistent in nature and does not decay over time.

7.2. Scaling with Cluster Mass

The SPARC sample shows that the dynamic factor $D = g_{\rm obs}/g_{\rm bar}$ converges toward 1 with increasing radius. On galactic scales, coherent field organisation is spatially limited.

Galaxy clusters are not directly included in this analysis. The following argument is therefore an extrapolation of the mechanism observed on galactic scales to larger systems.

When many saturated structures act together spatially, their field deformations superpose. The resulting total field tension at cluster level should reach a higher absolute level than on galactic scales,

 doi:10.20944/preprints202604.0640.v1

even if the relative amplification per individual system is weaker. This would be a natural explanation for why galaxy clusters show stronger gravitational lensing signals than expected from their visible mass alone.

Note on data availability: A direct test of this extrapolation requires lensing and gas data at cluster level. The original data from Clowe et al. (2006) were requested from the first author. No reply had been received by the time this manuscript was completed. Once these data are available, the mechanism can be tested quantitatively.

7.3. Connection to the Bullet Cluster

The Bullet Cluster illustrates this mechanism under dynamic conditions. During the collision of two clusters, the accumulated field tension remains bound to the coherent galaxy structures. The hot gas loses its coherent field coupling through dissipative processes. The spatial separation between gas centre and κ-peaks is therefore not evidence for a separate matter component, but a consequence of the different coupling strengths of coherent and diffuse structures to the field medium.

7.4. Prediction for Further Cluster Systems

If accumulation is a general principle, merging clusters should show systematically larger offsets between gas and lensing signal than relaxed clusters. Relaxed clusters have had time to adjust their field organisation, while during a merger the decoupling between gas and coherent field structure becomes directly visible.

This prediction is in principle testable on systems such as El Gordo or MACS J0717, which show collision geometries similar to the Bullet Cluster.

8. The Dark Matter Effect as a Consequence of Structure-Dependent Field Organisation

In standard cosmology, the dark matter effect is a residual quantity: the difference between the observed gravitational effect and the contribution of visible matter. In the UQSH, it is not a residual, but a direct consequence of the described field processes.

8.1. Three Sources of the Effect

The present analysis identifies three structurally distinct sources of the additional gravitational effect.

The first source is local field amplification by baryonic structures. Compact, coherent systems such as dwarf galaxies generate a strong relative field response. The median dynamic factor in the peak regime is $D \approx 2.15$, at a median baryonic mass of $7.35 \times 10^9\, M_\odot$.

The second source is large-scale field accumulation in massive systems. Diffuse spiral galaxies reach a higher absolute field level, even though the relative amplification is weaker at $D \approx 1.34$. Saturation occurs there over larger spatial scales.

The third source is collective accumulation in clusters. Many saturated structures together generate a large-scale field tension that systematically raises the lensing signal above the baryonic expectation.

8.2. The Instability Boundary as a Natural Upper Limit

The empirically determined instability boundary at approximately 50–80 kpc sets a natural spatial limit on coherent field organisation. Below it, the field accumulates coherent tension with measurable amplification. Above it, the field tension disperses and the relative excess dynamics converges to zero.

This boundary explains why the dark matter effect does not grow arbitrarily large. No observed system shows $D \gg 10$. The empirical upper limit lies at approximately $D_{\max} \approx 8$–10 in the 95th percentile of the SPARC sample.

 doi:10.20944/preprints202604.0640.v1

8.3. A Unified Explanation of Known Anomalies

Structure-dependent field organisation explains several known observational anomalies from a single principle.

Flat rotation curves arise from the redistribution of accumulated field tension into the outer radial regions below the instability boundary. The Radial Acceleration Relation follows as a statistical mean across systems of different regimes. The observed exponent of ≈0.67 corresponds to the mixture of saturated peak systems and non-saturated diffuse systems, as shown in Figure 7.

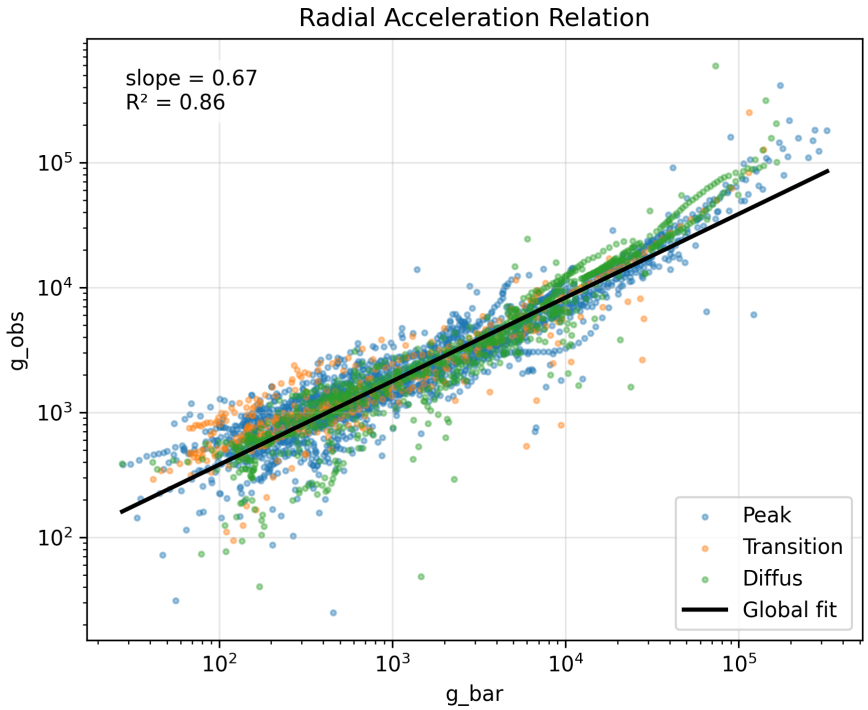

Figure 7. Power-law fit of the excess acceleration $g_{\mathrm{add}} \propto g_{\mathrm{bar}}^{n}$ for all analysed SPARC galaxies. The fitted exponent is $n \approx 0.67$ ($R^2 = 0.86$), consistent with a mixture of saturated peak systems and non-saturated diffuse systems in the UQSH framework.

The Bullet Cluster shows the spatial decoupling between coherent field structure and dissipative gas under dynamic conditions.

8.4. What This Approach Does Not Claim

The UQSH does not claim that dark matter is disproven. It shows that the observable phenomena are ontologically ambiguous, and that a field-mechanical interpretive framework can account for the same data with fewer categorical assumptions.

A closed dynamical derivation of all described effects from the field equation remains for future work. This work understands itself as a data-driven analysis with field-mechanical interpretation, not as a complete theory.

9. Physical Interpretation

9.1. Field-Based Reading of the Regime Structure

The observed regimes are interpreted as expressions of different organisational modes of the underlying field medium.

9.1.1. Peak Regime: Localised Reorganisation

The peak regime is the signature of a localised reorganisation dynamics of the field. The baryonic structure forms an organisational core that induces additional field organisation in the intermediate

 doi:10.20944/preprints202604.0640.v1

radial region. Its characteristic scale is set by an intrinsic reorganisation length ℓ_{reorg}. The scale parameter q then corresponds approximately to:

$$q \sim \frac{\ell_{\text{reorg}}}{R_{\text{system}}}. \tag{18}$$

For $q \approx 0.7$, this means the reorganisation length is about 70% of the system size, leading to a clearly localised structure with a pronounced peak.

9.1.2. Diffuse Regime: Large-Scale Field Response

The diffuse regime is the expression of a large-scale field response without local reorganisation. The field response spreads over a much larger scale without concentrating on a characteristic reorganisation length. The effective excess dynamics is distributed over a large radial range. The large value $q \approx 3.0$ suggests that the effective reorganisation length well exceeds the system size, giving rise to a broadly distributed, diffuse profile.

9.2. Conceptual Framing of the Dark Matter Effect

The dark matter effect is understood not as an expression of an additional matter component, but as a consequence of the field-mechanical organisation of physical space itself.

Physical space is described as a continuous, dynamic field medium whose local organisational state is characterised by a field $\phi(\mathbf{x}, t)$. Gravitational effects follow from spatial gradients of this field state and are not restricted to bound matter — they arise fundamentally with any form of field excitation. Bound field organisation appears as stable matter structure; free field excitation propagates dynamically through the medium and is phenomenologically observed as radiation. Neither represents a separate physical entity — both are different organisational states of the same underlying field medium.

9.2.1. Persistent Field Organisation as the Origin of the Dark Matter Effect

Free field excitations generate real deformations of the field medium that are not strictly local and do not instantaneously relax. In astrophysical systems, the continuous generation of such excitations leads to a permanent superposition of field deformations. A substantial fraction of these superpositions does not form stably bound states, yet remains field-mechanically active. The resulting large-scale, persistent field organisation manifests macroscopically as the dark matter effect.

9.2.2. Baryonic Structure as Source and Anchor

Baryonic structures play a dual role. Radiation-active systems such as stars act as continuous sources of free field excitation. Radiative processes continuously generate deformations of the field medium and thereby contribute directly to large-scale field organisation. At the same time, baryonic structures represent stable, bound organisational states of the field and act as local anchor regions of the field structure. They generate a spatial pre-stress of the field medium that enables and stabilises the superposition, coherence, and persistence of field deformations.

The dark matter effect arises from the interplay of continuous field excitation and its structural stabilisation through baryonic organisation. It is therefore systematically coupled to baryonic structure without being caused by it alone.

9.2.3. Non-Coupling Field Organisation and Observability

Non-coupling field organisation is not to be understood as non-existent or physically inert, but simply as not directly visible in the relevant observational regime. Such states still contribute to the overall organisation of the field medium and possess gravitational effect. The dark matter effect can therefore be understood as the macroscopic action of those field portions that do not appear as visible, stably bound matter structures, yet still generate persistent deformations and tension states in the field.

 doi:10.20944/preprints202604.0640.v1

The so-called dark matter halo corresponds in this interpretation not to a particle reservoir, but to a metastable state of large-scale field organisation.

9.3. Interpretation within the UQSH Framework

The observed regimes can be linked to different coupling and organisational states of the field medium. The UQSH postulates a field equation of the form:

$$\partial_t \phi + v[\phi] \cdot \nabla \phi = \nu \Delta \phi + \gamma \nabla \cdot \left[\sigma\left(\frac{|\nabla \phi|}{S_H} \right) \frac{\nabla \phi}{\sqrt{\varepsilon^2 + |\nabla \phi|^2}} \right] + \kappa R[\phi] - \mu \phi, \tag{19}$$

where $\sigma(z)$ describes an activation function (e.g. $\sigma(z) = z^m/(1+z^m)$), S_H is a characteristic saturation scale, and $R[\phi]$ is a non-local reorganisation term.

9.3.1. Coupling and Threshold Crossing

Localised reorganisation is only activated above a critical threshold:

$$|\nabla \phi| \geq S_{\text{crit}}. \tag{20}$$

In the peak regime, the baryonic structure leads to a local field organisation that exceeds this threshold. The reorganisation term $R[\phi]$ is activated and generates a localised additional field structure with a characteristic length scale. In the diffuse regime, the threshold is not reached or only weakly so; the reorganisation remains large-scale and diffusely distributed.

9.3.2. Scale Analogy of Localised Coupling Modes

The peak regime can be interpreted as the expression of a localised, coupling-capable field mode. This allows a cross-scale analogy between microscopic and galactic organisational forms. Stable, coupling-capable field modes at the microscopic scale take the role of electrons in a bound system; at the galactic scale, dwarf galaxies and satellite systems appear as analogous bound substructures of a central galactic field node. The structural correspondence

$$\text{Electrons} \longleftrightarrow \text{Dwarf galaxies}$$

is not to be understood as an identity of physical forces, but as an analogy of organisational form. In both cases, the number of stably bound substructures is determined not merely by their existence, but by their capacity to couple to the central field structure. This analogy is intended as a structural heuristic and requires independent theoretical elaboration.

9.4. Interpretation of the Transition Zone

The sparsely populated but real transition zone $1.2 < q < 2.5$ suggests a dynamically less favoured state. Two physical interpretations are conceivable.

9.4.1. Preferred Field Modes

By analogy with discrete quantum states, the observed main regimes might correspond to preferred organisational modes of the field medium. Several dynamically preferred field configurations exist; the transition zone is energetically less favourable, and systems preferentially relax into one of the more stable modes. This is analogous to phase transitions in statistical physics, where systems preferentially remain in defined phases while transition states occur more rarely.

9.4.2. Dynamic Transition

Alternatively, the transition zone might in principle be accessible, but with a shorter characteristic lifetime. Systems can pass through the transition zone, but the dwell time is short compared to the

 doi:10.20944/preprints202604.0640.v1

dominant regimes, reducing the probability of observing a system in this state. From the observed frequency, a rough upper bound on the transition time can be estimated:

$$\tau_{\text{trans}} \approx \frac{n_{\text{trans}}}{n_{\text{total}}} \times \tau_{\text{regime}} \approx 0.12 \times 10\,\text{Gyr} \sim 1.2\,\text{Gyr}. \tag{21}$$

This is of an order of magnitude compatible with slow dynamical reorganisation processes of galactic systems.

9.5. Coupling to Baryonic Structure

The systematic dependence of the regime structure on the baryonic scaling parameter a shows that the excess dynamics is not independent of visible matter. This is consistent with the empirically observed tight coupling between baryonic and dynamical acceleration, as visible in the Radial Acceleration Relation [1].

Baryonic structures are not only local organisational cores of the field, but simultaneously sources of ongoing field excitation and anchors of its large-scale stabilisation. More concentrated baryonic distributions (high a) lead to large-scale diffuse field response; less concentrated distributions (low a) favour the formation of localised reorganisation. Strongly concentrated baryonic structures already saturate the local field organisation, so that additional reorganisation can only occur at large scales.

9.6. Inner Structure and the Core-Cusp Problem

9.6.1. Inner Slopes of the Mass Distribution

To investigate the inner structure of galactic rotation profiles, logarithmic slopes of the effective mass distribution $M(r) \sim r^{\alpha}$ were determined from the five innermost data points. The resulting values span a broad range from $\alpha \approx 0.6$ to 3.8, with an overall median of $\alpha \approx 2.1$.

An NFW profile corresponds to $\alpha = 2$ in the mass scale, a flat core profile to $\alpha = 3$. The measured values thus lie predominantly near the NFW expectation, but show a systematic dependence on system size that is described below.

The inner slope determination was performed for different numbers of inner data points ($n = 3, 5, 8$). The resulting distributions show high consistency; median values and scatter remain nearly unchanged. A significant dependence of the inner slope on the q-regime alone is not apparent. The inner dynamics is not primarily determined by local structural parameters, but by the global system size.

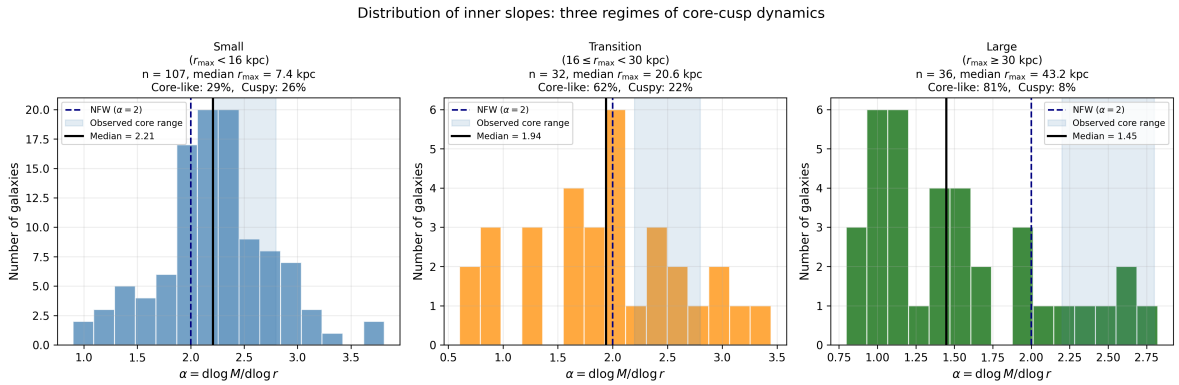

Figure 8. Distribution of inner slopes α for the three size regimes. Left: small systems ($r_{\text{max}} < 16\,\text{kpc}$), centre: transition systems ($16 \leq r_{\text{max}} < 30\,\text{kpc}$), right: large systems ($r_{\text{max}} \geq 30\,\text{kpc}$). The dashed line marks the NFW expectation ($\alpha = 2$); the shaded band indicates the observed core region. Large systems are predominantly core-like (81%), while small systems show a broad distribution with no dominant regime.

 doi:10.20944/preprints202604.0640.v1

9.6.2. System Size as the Primary Driver

A direct analysis of the inner slope α as a function of the maximum rotation curve radius $r_{\max}$ yields a statistically highly significant negative correlation across the full sample: $r = -0.46$, $p < 0.0001$.

This finding may appear counterintuitive at first, since the standard literature identifies small dwarf galaxies as the archetypal examples of core structures. The difference lies in the quantity being measured: the slopes α determined here describe the logarithmic slope of the effective mass distribution $M(r) \sim r^{\alpha}$, not the density distribution $\rho(r)$ directly. A flat mass profile in the sense of $\alpha < 2$ means that the enclosed mass grows more slowly than r^2, indicating an outwardly declining effective mass density. That is not the same as a classical core profile in the density.

This finding deserves to stand on its own. The classical core-cusp problem in astronomy focuses on small dwarf galaxies that observationally often show flat density profiles, while CDM simulations predict steep cusps there. The present analysis reveals an independent pattern: in the mass distribution $M(r)$, it is the large systems that systematically show flatter inner profiles.

This is not a contradiction of the literature, but a complementary finding. Small dwarf galaxies show cores in the density distribution because baryonic feedback processes or field-mechanical effects flatten the central density. Large systems show cores in the mass distribution because the accumulated large-scale field tension mechanically widens the centre. These are two different mechanisms producing the same signature in different size regimes.

Within the UQSH framework, this is a natural consequence of the saturation dynamics: the larger a system, the more strongly the field resists further local concentration. The result is not coincidental and is not an artefact of data processing. It is a direct expression of the structure-dependent field organisation that forms the central theme of this work.

Small dwarf galaxies show a broad scatter in this analysis with a median near the NFW expectation ($\alpha = 2.21$). This does not mean they have no cores, but that their inner mass distribution is on average not flatter than NFW. The cores in dwarf galaxies reported in the literature typically refer to the density, while here the mass distribution is analysed. Both quantities are consistent with each other, but describe different aspects of the inner structure.

Larger systems show systematically flatter, i.e. more core-like, inner profiles.

The sample can be divided into three clearly distinguishable regimes on the basis of this finding, which are statistically separable from one another (Kruskal-Wallis $H = 33.1$, $p < 0.0001$; pairwise Mann-Whitney $p < 0.03$ in each case):

Small systems with $r_{\max} < 16$ kpc show a median of $\alpha = 2.21$ and broad scatter. 29% are core-like ($\alpha < 2.0$), 26% show cuspy-like behaviour ($\alpha > 2.5$). The correlation between $r_{\max}$ and α is not significant there ($r = -0.08$, $p = 0.42$). System size alone does not explain the inner slope in this range.

Systems in the transition zone with $16 \leq r_{\max} < 30$ kpc show a median of $\alpha = 1.94$, right at the NFW boundary. 63% are core-like, only 22% cuspy. The correlation between $r_{\max}$ and α is there practically zero ($r = +0.08$, $p = 0.67$), suggesting a coexistence of both mechanisms.

Large systems with $r_{\max} \geq 30$ kpc show a median of $\alpha = 1.45$. 81% are core-like, only 8% cuspy. The correlation is significant there ($r = -0.38$, $p = 0.02$). System size clearly dominates the inner structure.

 doi:10.20944/preprints202604.0640.v1

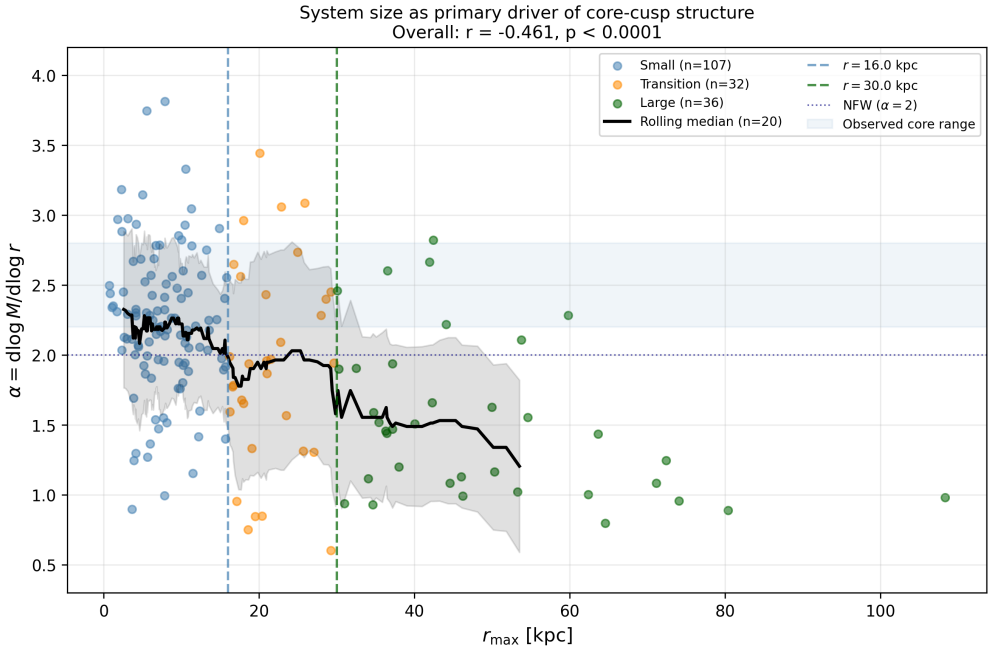

Figure 9. System size as the primary driver of core-cusp structure. Inner slope $\alpha = \mathrm{d}\log M/\mathrm{d}\log r$ as a function of the maximum rotation curve radius $r_{\max}$ for all analysed SPARC galaxies. Small systems ($r_{\max} < 16$ kpc, blue), transition systems ($16 \leq r_{\max} < 30$ kpc, orange), and large systems ($r_{\max} \geq 30$ kpc, green). The running median (black line, $\pm 1\sigma$ band) shows a systematic decrease of α with system size ($r = -0.46$, $p < 0.0001$). Large systems are predominantly core-like; small systems show a broad distribution with no clear size dependence.

9.6.3. Connection to the RAR

Galaxies with different inner profile shapes systematically lie on the same global acceleration relation. Figure 10 shows the RAR colour-coded by inner structural class. Core-like systems ($\alpha < 1.7$), intermediate systems ($1.7 \leq \alpha \leq 2.3$), and cuspy-like systems ($\alpha > 2.3$) are not separated from each other, but follow the same global relation. The RAR is therefore a universal relationship that holds independently of the specific inner mass distribution.

The combined view of RAR and inner structure leads to a consistent picture. The RAR appears as a global constraint on the dynamics that follows from the cross-scale organisation of the underlying field. The inner structure, by contrast, reflects local equilibrium states between field organisation, system size, and continuous reorganisation, as shown in Section 9.6.4.

 doi:10.20944/preprints202604.0640.v1

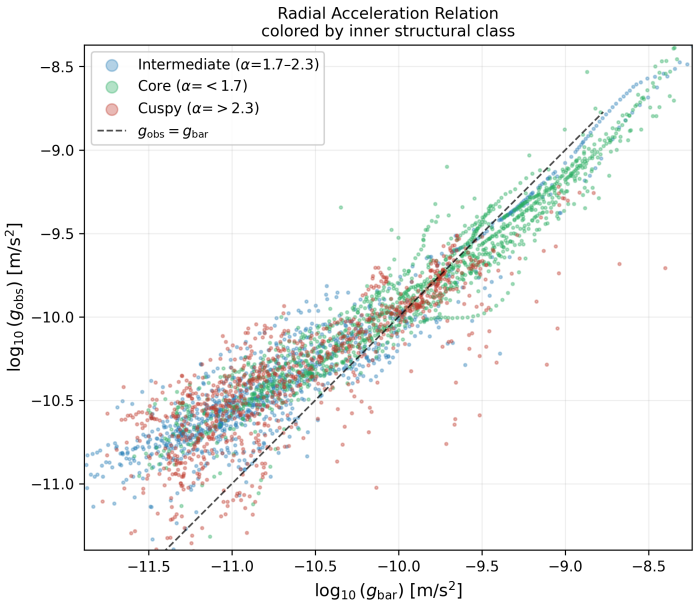

Figure 10. Radial Acceleration Relation colour-coded by inner structural class. Core-like ($\alpha < 1.7$), intermediate ($1.7 \leq \alpha \leq 2.3$), and cuspy-like ($\alpha > 2.3$) systems lie on the same global relation. No separation by inner profile shape is apparent.

9.6.4. Three Regimes of Core-Cusp Dynamics

Terminological note: The term "gamma radiation" in this section is not used in the classical astrophysical sense of high-energy photons, but as a label for high-frequency tension fronts in the continuous field medium of the UQSH. These arise at locations of maximum local field saturation and propagate through the medium analogously to electromagnetic gamma radiation, yet are ontologically distinct: they are deformations of the field medium itself, not particles or photons. The analogy concerns the form of propagation and the energy density, not the particle nature.

The observed size dependence can be explained within the UQSH framework through two physically distinct mechanisms whose relative contribution varies with system size.

In small systems, the field medium still has tolerance. The large-scale field tension is weak enough that local processes co-determine the inner structure. There, gamma radiation plays an active role: it arises as a higher-frequency tension front at locations of high local field saturation, propagates spherically, and is focused by pressure at relief channels. This radiation is coupled to the baryonic anchor matter that pre-stresses and stabilises the field. The intensity of the gamma radiation decreases with growing distance from the anchor matter. It saturates the field in the central region and prevents the formation of a strongly cuspy profile there. Without baryonic anchor matter, no pronounced DM halo forms, because the field organisation is not stabilised. Tests show that 93–99% of gamma corrections in small systems are core-forming.

In the transition zone between 16 and 30 kpc, both mechanisms are equally active. System size begins to dominate the field organisation, but the gamma mechanism is not yet suppressed. The inner slope scatters broadly and shows no clear correlation with $r_{\max}$. This region corresponds to the separation point of the two regimes.

The question of why nature switches precisely around 16–30 kpc is not trivial. In the present analysis, this threshold was determined empirically: the running median of the inner slope falls below the NFW boundary $\alpha = 2$ at $r_{\max} \approx 16$ kpc, and the correlation between $r_{\max}$ and α only becomes significant from $r_{\max} \approx 30$ kpc onward. The transition zone is therefore not an arbitrary choice, but follows directly from the data.

A physical derivation of these scales from fundamental parameters of the Qu-foam is still outstanding. Within the UQSH framework, it is natural to link the threshold to the characteristic coherence length of the field — the scale below which local field organisation is possible and above which large-

 doi:10.20944/preprints202604.0640.v1

scale field tension dominates. This coherence length should be derivable from the field equation and might be connected to known galactic scales, such as the typical scale length of baryonic discs or the characteristic range of field-mechanical reorganisation. This is a concrete open question to be addressed in future work.

In large systems, the field has reached its maximum organisational capacity within the given regime. The large-scale field tension is so strong that it suppresses the gamma contribution and dominates the inner structure. The field resists further concentration, which manifests directly as a flat inner profile. The larger the system, the stronger this effect. That is why 81% of large systems are core-like, without any explosive feedback process being required.

This interpretation simultaneously explains the finding of [4,11] that the core radius correlates with the disc scale length. In the UQSH this correlation is natural: the gamma radiation arises from the baryonic structure itself, so its characteristic range is directly coupled to the disc size.

9.6.5. The Interplay of Gamma Radiation and Non-Coupling Field Organisation

At first glance there seems to be a contradiction: gamma radiation is coupled to baryonic anchor matter and acts locally in a core-forming way. The dark matter effect, on the other hand, arises from non-coupling field organisation that is not directly bound to baryons. How do these two relate?

The key lies in the saturation of the field medium. Gamma radiation modulates the local saturation state of the field. Where field tension is raised by gamma radiation, the medium approaches its local saturation boundary more quickly. Above this boundary, the field can no longer absorb additional local tension and redistributes the excess outward. This redistribution process is what generates and stabilises the large-scale non-coupling field organisation.

Gamma radiation is therefore not the cause of the dark matter effect, but a modulator of the local field structure. It co-determines whether the field medium is locally saturated and thereby organises itself at large scales. In small systems, this local modulation effect dominates. In large systems, the large-scale field tension is already so strong that it suppresses the gamma radiation and determines the inner structure itself.

The peak regime and the diffuse regime are thus two different responses of the same field medium to the same question: how does the field organise itself when baryonic matter continuously generates field excitation? The answer depends on whether the local saturation boundary is exceeded or not.

9.6.6. Saturation Behaviour and Non-Local Extensions

The excess acceleration $\Delta g = g_{\mathrm{obs}} - g_{\mathrm{bar}}$ shows no divergent behaviour, but a only weakly rising and then flattening development. Δg remains within a limited range of values, consistent with a saturation dynamics of the underlying field.

However, Δg does not reach a plateau even in the low-g regime, but continues to scale with g_{bar}. The described excess dynamics alone therefore does not produce a complete flattening of the inner mass distribution.

As a test, a non-local extension in the form of a gradient term was introduced:

$$\Delta g_{\mathrm{new}}(r) = \Delta g(r) + \lambda \frac{d}{dr}(r \cdot \Delta g(r)). \tag{22}$$

This term describes an effective radial redistribution of the excess dynamics and can be interpreted as an analogue of a field flux or tension relaxation. First tests show that such non-local contributions contribute considerably more strongly to the formation of core-like profiles than purely local saturation effects.

The parameter λ has the dimension of a length. In first tests it was linked to the disc scale length R_{disk} of the respective galaxy, i.e. $\lambda \sim R_{\mathrm{disk}}$. This is natural because the gamma radiation arises from the baryonic structure itself, so its range should be coupled to the size of the disc. In this sense the term does not describe a free adjustment, but a physically motivated radial redistribution of the excess

 doi:10.20944/preprints202604.0640.v1

dynamics on the scale of the baryonic source. A complete derivation of λ from the UQSH field equation remains for future work.

Note: These non-local extensions and the quantitative modelling of the gamma saturation term are exploratory and preliminary. A complete physical derivation within the UQSH framework remains for future work.

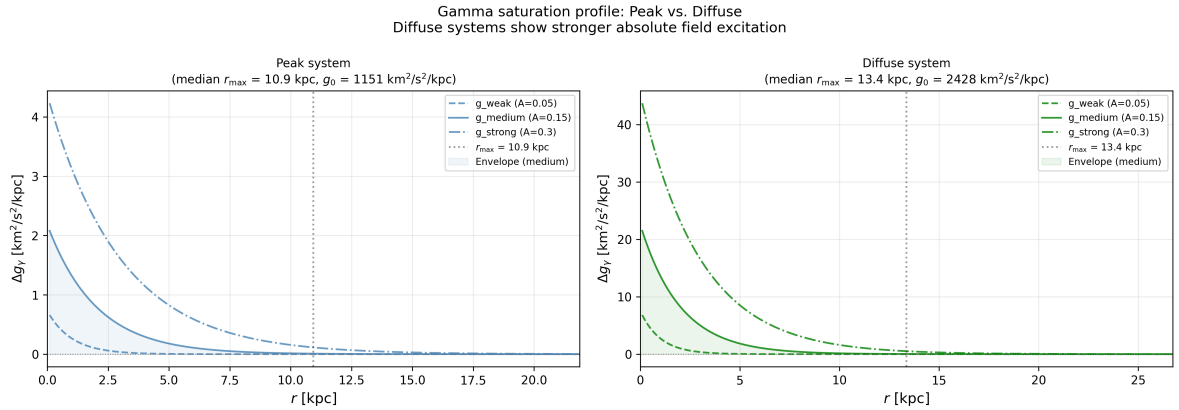

Figure 11. Gamma saturation profile for median peak and diffuse systems. Three gamma term strengths are shown (weak, medium, strong). Diffuse systems have a larger median $r_{\max}$ and show stronger absolute field excitation. The dashed vertical line marks the median $r_{\max}$ of the respective regime; the shaded area shows the mean envelope.

In the UQSH, no static background state exists. All observable structures are dynamic organisational states of a continuous field whose local configurations continually reorganise. Even on small scales, no completely resting states exist. The dynamics continues across scales and prevents an unlimited local concentration of field organisation.

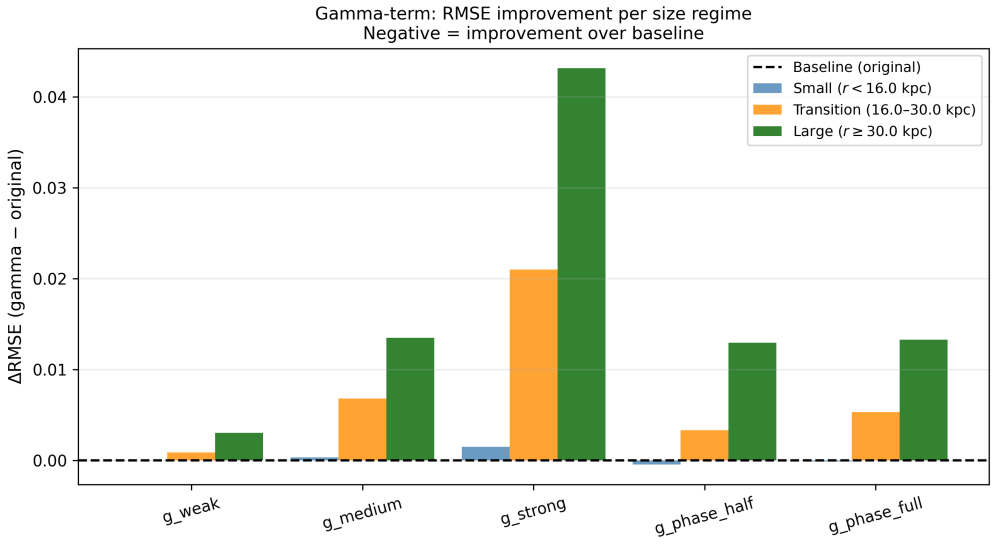

Figure 12. RMSE improvement of the gamma saturation term relative to the baseline for each size regime. Negative values indicate improvement. Small systems show the strongest response to the gamma correction; large systems are dominated by the global field tension and show virtually no response.

9.7. Implications for the Bullet Cluster

9.7.1. UQSH Interpretation

The Bullet Cluster is considered one of the strongest empirical arguments for a separation between baryonic matter and gravitationally effective mass. Gravitational lensing analysis shows that the mass distribution follows the galaxies rather than the dominant baryonic gas component.

 doi:10.20944/preprints202604.0640.v1

In the UQSH, the Bullet Cluster is interpreted not as a separation between baryonic and non-baryonic substance, but as a separation between different organisational and coupling states of the same continuous field. While the hot gas responds strongly dissipatively during the collision, galaxies as more coherent field structures largely retain their effective gravitational organisation. The observed shift between the gas maximum and the lensing signal follows directly from structure-dependent, non-local field dynamics.

9.7.2. Quantitative Comparison

The distances of the lensing proxy maxima to the gas maximum as well as to the galaxy centres were extracted from the calibrated image of [3]. The 200 kpc scale bar served as the reference for pixel calibration.

The measured offsets between the gas maximum and the two κ-peaks are 218.7 kpc and 227.6 kpc, with a mean of $\sim$223 kpc. The UQSH field model was applied to the Bullet Cluster geometry. The effective field follows as a weighted superposition of a coherent galaxy component and a diffuse gas component with reduced field coupling. The κ-map follows from the negative Laplacian of the total field, projected along the line of sight.

The model reproduces offsets of 219 kpc and 200 kpc, with a mean of $\sim$210 kpc [3,12]. The deviation of about 6% from the observed mean of 223 kpc is consistent with the simplified geometry of the model, which was not calibrated to the real Clowe configuration.

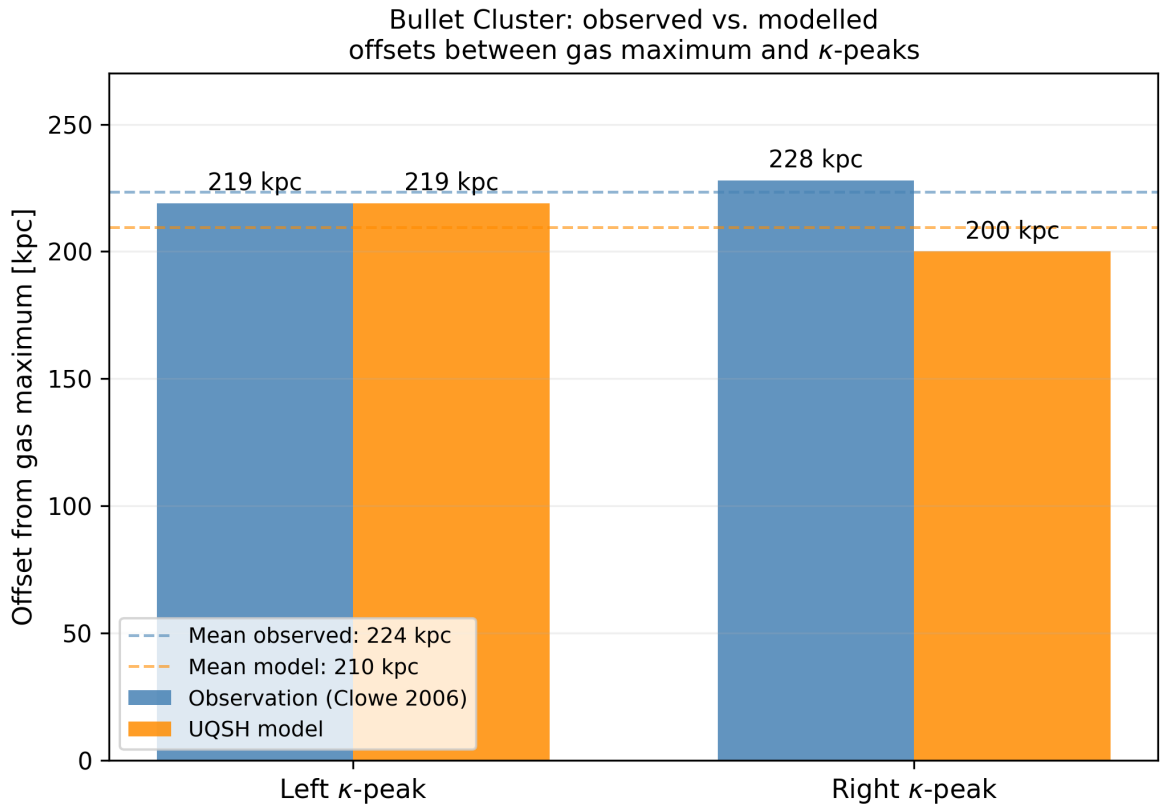

Figure 13. Comparison of measured and modelled offsets between the gas maximum and κ-peaks in the Bullet Cluster. Left: observed offset 219 kpc, UQSH model 219 kpc. Right: observed offset 228 kpc, UQSH model 200 kpc. The model reproduces the observed left-peak offset of 219 kpc within the typical measurement precision of weak-lensing analyses, without requiring free parameters for a dark matter distribution. The right peak lies about 12% below the observed value, consistent with the simplified geometry of the model. The model reproduces the characteristic order of magnitude of the separation without any free adjustment to the observational data.

The spatial situation is shown in Figure 6. The UQSH model reproduces the characteristic separation between the gas centre and κ-peaks without an additional non-baryonic matter component.

 doi:10.20944/preprints202604.0640.v1

9.8. Testable Predictions

9.8.1. Galaxy Evolution and Regime Transitions

If the observed regimes represent developmental stages or different formation pathways, peak and diffuse systems should differ systematically in further observational quantities: gas fraction and star formation rate, surface brightness, internal kinematic order, and degree of perturbation.

9.8.2. Spatial Distribution of Subsystems

If peak structures are associated with a more advanced developmental stage or greater decoupling from the host system, peak systems should on average lie at larger distances from their host galaxies than diffuse dwarf systems. This hypothesis can be empirically tested by correlating the projected distance to the respective host galaxy with the regime classification for satellite and dwarf galaxies.

Preliminary analysis. The present evaluation is based on angular distances as a proxy for environmental distance. A more detailed analysis using three-dimensional distances and confirmed group memberships is the subject of future work.

To investigate a possible environmental dependence, a first assignment between low-mass dwarf galaxies and nearby massive host galaxies was performed. The resulting angular distances show a systematic difference between the dynamical regimes. Diffuse systems occur over a broad range of distances, including very small angular separations (5°). Peak systems, by contrast, are not found at very small separations but occur preferentially at intermediate to larger angular distances (∼7°–25°).

Distance alone is insufficient to uniquely determine the dynamical regime. Systems at comparable angular distances can show both diffuse and peak behaviour. This analysis is preliminary, but provides a first empirical hint of a correlation between dynamical regime and environmental distance.

9.8.3. Temporal Evolution

The UQSH interpretation implies a causal delay in field reorganisation:

$$\tau \sim \frac{L}{c_{\mathrm{eff}}}, \tag{23}$$

where L is a characteristic length scale and $c_{\mathrm{eff}} \leq c$ is an effective reorganisation velocity. Changes in the baryonic mass distribution therefore do not instantaneously lead to a complete adjustment of the non-coupling field structure.

10. Comparison with Standard Models

10.1. Expectations from the ΛCDM Model

In the ΛCDM model, the observed excess term is interpreted as the contribution of a dark matter halo. The density profiles of such halos — for instance NFW or Burkert profiles — form a continuous family described by a few parameters. This implies that the resulting rotation curves should exhibit a continuous variety of shapes, with no preferred structural states. A continuous halo model would predict a more uniform distribution of the scale parameters q across the entire value range.

10.2. Observed Discrepancy

The present data show a clear concentration in two preferred regions ($q \approx 0.7$ and $q \approx 3.0$), alongside a real but more sparsely populated transition zone. This structure is not the natural expectation of continuous halo models and calls for a deeper explanation. The results extend the known coupling between baryonic and dynamical structure — as visible in the Radial Acceleration Relation — with additional information about the shape of the excess dynamics.

10.3. Possible Explanation within the ΛCDM Framework

Structural differences of this kind could in principle be explained within the standard model through baryonic processes: feedback mechanisms such as stellar winds, supernova outbursts, and

 doi:10.20944/preprints202604.0640.v1

AGN activity; different formation and evolutionary histories; and morphological differences between spiral and dwarf galaxies. However, this would require additional assumptions. Why do these processes lead to preferred regions of parameter space? Why is the transition zone systematically less populated? Why is there such a strong type dependence within the regimes? The observed concentration of systems in preferred parameter regions demands, within the baryonic feedback framework, an explanation for the reduced population of the transition zone. A detailed investigation of these questions through simulations with baryonic physics remains for future work.

10.4. Distinguishing between the Approaches

The field-based interpretation differs from the standard model in several testable respects, summarised in Table 3.

Table 3. Comparison of model predictions for the observed regime structure.

Observable	ΛCDM	UQSH
Number of preferred regimes	continuous	preferred modes
Distribution of q values	smooth	bimodal with transition zone
Dependence on a	weak (indirect)	systematic (direct)
Coupling to baryons	via feedback	fundamental coupling
Spatial correlation	no clear expectation	peak systems more distant
Temporal delay	instantaneous	causally bounded

11. BTFR: Comparison of V_{out} and V_{flat}

Two velocity definitions were compared in the baryonic Tully-Fisher relation (BTFR) [8,9]: the classical flat rotation velocity V_{flat} and a structurally defined outer velocity V_{out}, computed as the median of the three outermost data points of the rotation curve.

The analysis was performed on 102 galaxies for which both V_{flat} and V_{out} were reliably determinable. For this subsample, V_{out} yields a small but consistent improvement over V_{flat}: the scatter of the BTFR residuals drops from $\sigma_{\mathrm{flat}} = 0.222$ dex to $\sigma_{\mathrm{out}} = 0.220$ dex, corresponding to a reduction of about 1%.

For galaxies without a clearly defined asymptotic behaviour, V_{flat} is not reliably determinable. In such cases V_{out} does yield a measurement, but it reflects a dynamics that has not yet concluded. Including these systems cancels the improvement, because the outermost data points there do not represent a characteristic value.

This result is consistent with the regime structure of the paper. Peak systems typically show no pronounced asymptotic behaviour, which makes V_{flat} harder to determine for them. Diffuse systems with a well-developed flat rotation curve are well captured by V_{flat}, while V_{out} works equally well there because both definitions converge for such systems.

The choice of a characteristic velocity is therefore not a universal question, but depends on the dynamical state of the galaxy. The peak regime and the diffuse regime place different demands on the velocity definition, which explains the observed regime-dependent precision of the BTFR.

12. Discussion, Conclusions, and Outlook

12.1. Main Results

This work presents a systematic analysis of galactic rotation curves from the SPARC database. The empirically extracted excess term $C(r) = v_{\mathrm{obs}}^2 - v_{\mathrm{bar}}^2$ shows, after normalisation, a consistent structure of preferred regimes. Global fits over subsamples identify two dominant dynamical regimes: the peak regime with $q \approx 0.5$–1.0 and the diffuse regime with $q \approx 3.0$. Complementary individual fits show a distribution of about 62% peak systems, 12% transition systems, and 26% diffuse systems. The regime structure depends systematically on the baryonic scaling parameter a, pointing to a fundamental coupling to baryonic structure. Within each regime, a universal shape function is apparent with low scatter (MSE ≈ 0.016–0.13).

 doi:10.20944/preprints202604.0640.v1

The analysis is based on the SPARC database, which represents one of the most extensive and homogeneous samples of galactic rotation curves. A verification of the results on independent datasets remains the subject of future work.

12.2. Interpretation and Significance

The observed structure with two preferred regions and a more sparsely populated transition zone is not the natural expectation from continuous halo models. It points to preferred dynamical states. This work understands itself primarily as a data-driven analysis with phenomenological interpretation. A complete theoretical derivation of the observed structures remains for future work.

The observed regimes are interpreted as expressions of different organisational modes of the underlying field medium: the peak regime corresponds to a localised reorganisation dynamics with a characteristic length scale; the diffuse regime corresponds to a large-scale field response without local reorganisation. The reduced population of the transition zone can be interpreted analogously to phase transitions or discrete quantum states, where preferred configurations exist while transition states are dynamically less stable or energetically less favourable.

12.3. Open Questions and Future Work

Despite the clear empirical structure, several questions remain open.

12.3.1. Physical Derivation of the Shape Function

The parametric form $F(x) = x^p e^{-x/q} / \max(\cdots)$ was determined empirically. A quantitative derivation of this form from an underlying field equation is still outstanding. In particular, it remains to be clarified which field equation leads to the observed values $p \approx 1.2$ and $q \approx 0.7$ or $q \approx 3.0$, and whether these parameters can be derived from fundamental field constants.

12.3.2. Scaling Relations

The dependence of the parameters $C_{\max}$ and R on the baryonic mass should be systematically investigated. First analyses suggest scaling relations of the form

$$C_{\max} \propto M_{\mathrm{bar}}^{\alpha}, \qquad R \propto M_{\mathrm{bar}}^{\beta} \tag{24}$$

with $\alpha \approx 0.5$ and $\beta \approx 0.3$. A quantitative confirmation of these relations and their physical interpretation remains to be established.

12.3.3. Spatial Correlations

The prediction that peak systems on average lie at larger distances from their host galaxies than diffuse dwarf systems can be further tested empirically. A corresponding analysis requires the identification of host-satellite pairs in the SPARC sample, the determination of projected and ideally three-dimensional distances, and a statistical correlation analysis with the regime classification.

12.3.4. Extension to Other Observables

The present analysis focuses on rotation curves. An extension to other observables would be desirable. Can the preferred regimes also be identified in gravitational lensing signals? Is an analogous regime structure visible in the velocity dispersion of elliptical galaxies? Can analogous signatures be found in cosmological observations?

12.3.5. Comparison with Simulations

A quantitative comparison with numerical simulations is necessary. Do high-resolution ΛCDM simulations with baryonic physics reproduce the observed bimodal structure? Can simulations of the proposed field equation quantitatively reproduce the empirical shape functions?

 doi:10.20944/preprints202604.0640.v1

The observed ratio of peak to non-peak systems (62% : 38%) lies close to the golden ratio $\varphi \approx 1.618$, with a deviation of approximately 1.7%. Whether this reflects a deeper organisational principle of the field medium or is a statistical coincidence remains an open question that warrants investigation on larger samples.

12.4. Significance for the Understanding of Dark Matter

The present results show that the additional dynamics usually attributed to dark matter cannot be described by a completely smooth family of freely adjustable halo profiles. It takes on preferred structural states that are systematically coupled to baryonic structure. This opens the possibility of understanding galactic dynamics as an emergent phenomenon of a deeper, cross-scale organisation, rather than attributing it to an additional freely distributable matter component.

12.5. Conclusion

This work has presented a systematic analysis of 164 galactic rotation curves from the SPARC database. The empirically extracted excess term $C(r) = v_{\mathrm{obs}}^2 - v_{\mathrm{bar}}^2$ shows, after suitable normalisation, a consistent structure of preferred dynamical regimes. Global fits identify two dominant regimes: a peak regime with $q \approx 0.5$–1.0 and a diffuse regime with $q \approx 3.0$. The overall distribution is broader: about 62% of systems lie in the peak regime, about 26% in the diffuse regime, and about 12% in the transition zone. The underlying dynamics is not strictly bimodal, but shows two preferred states with a real transition zone.

The systematic dependence of the regime structure on the baryonic scaling parameter shows that the excess dynamics is fundamentally coupled to baryonic structure. In the UQSH, this dynamics is understood as the expression of persistent, not fully coupling-capable field organisation, generated and stabilised by baryonic structure and continuous field excitation. The peak regime corresponds to a localised reorganisation dynamics; the diffuse regime to a large-scale field response without local reorganisation.

The proposed interpretation leads to testable predictions, in particular regarding the spatial distribution of subsystems, the correlation with further physical properties, and a possible cross-scale analogy of localised coupling modes. This work thus represents an alternative perspective that attributes the observed discrepancy between visible and gravitational mass not to an additional particle component, but to the organisation of a continuous field medium.

Citation

Rexhepi, U. Q. (2026).
Bimodal Regime Structure in Galactic Rotation Curves.
Independent Researcher, Tübingen, Germany.
ORCID: https://orcid.org/0009-0003-4145-5431

GitHub (Analysis):
https://github.com/ukshinrexhepi-cloud/dm-effect-analysis

GitHub (UQSH):
https://github.com/ukshinrexhepi-cloud/Universelle-Quanten-Schaum-Hypothese-UQSH-

HAL: https://hal.science/PLACEHOLDER

Acknowledgments: The author thanks the scientific community for making the SPARC database publicly available [2], which forms a central foundation of this work. This work made use of the NASA/IPAC Extragalactic Database (NED), which is operated by the Jet Propulsion Laboratory, California Institute of Technology, under contract with the National Aeronautics and Space Administration. The Bullet Cluster analysis is based on HST ACS image data from the Hubble Legacy Archive (HLA), provided by the Space Telescope Science Institute (STScI) under NASA contract NAS 5-26555, Programme 10200 (PI: D. Clowe). This work has made use of observations made with the NASA/ESA Hubble Space Telescope. Parts of the data analysis were carried out using Python and publicly

 doi:10.20944/preprints202604.0640.v1

available scientific software libraries, including NumPy, SciPy, Pandas, and Matplotlib. AI-based tools were used in a supporting capacity at several stages of this work: in the structuring and editorial revision of the manuscript, in debugging and optimising analysis code, and in discussing physical interpretations and checking internal consistency. All scientific decisions, interpretations, and conclusions are the author's own. Responsibility for the content and methodology of this work lies solely with the author.

References

1. McGaugh, S.S.; Lelli, F.; Schombert, J.M. Radial Acceleration Relation in Rotationally Supported Galaxies. *Phys. Rev. Lett.* **2016**, *117*, 201101.
2. Lelli, F.; McGaugh, S.S.; Schombert, J.M. SPARC: Mass Models for 175 Disk Galaxies with Spitzer Photometry and Accurate Rotation Curves. *Astron. J.* **2016**, *152*, 157.
3. Clowe, D.; Bradač, M.; Gonzalez, A.H.; Markevitch, M.; Randall, S.W.; Jones, C.; Zaritsky, D. A Direct Empirical Proof of the Existence of Dark Matter. *Astrophys. J. Lett.* **2006**, *648*, L109–L113.
4. de Blok, W.J.G. The Core-Cusp Problem. *Adv. Astron.* **2010**, *2010*, 789293.
5. Navarro, J.F.; Frenk, C.S.; White, S.D.M. The Structure of Cold Dark Matter Halos. *Astrophys. J.* **1996**, *462*, 563.
6. Rubin, V.C.; Ford, W.K. Rotation of the Andromeda Nebula from a Spectroscopic Survey of Emission Regions. *Astrophys. J.* **1970**, *159*, 379.
7. Milgrom, M. A modification of the Newtonian dynamics as a possible alternative to the hidden mass hypothesis. *Astrophys. J.* **1983**, *270*, 365.
8. McGaugh, S.S. The Baryonic Tully-Fisher Relation of Gas-Rich Galaxies as a Test of ΛCDM and MOND. *Astron. J.* **2012**, *143*, 40.
9. Lelli, F.; McGaugh, S.S.; Schombert, J.M.; Pawlowski, M.S. One Law to Rule Them All: The Radial Acceleration Relation of Galaxies. *Astrophys. J.* **2017**, *836*, 152.
10. Zwicky, F. Die Rotverschiebung von extragalaktischen Nebeln. *Helv. Phys. Acta* **1933**, *6*, 110.
11. Oh, S.-H.; Hunter, D.A.; Brinks, E.; et al. High-Resolution Mass Models of Dwarf Galaxies from LITTLE THINGS. *Astron. J.* **2015**, *149*, 180.
12. Markevitch, M.; Gonzalez, A.H.; Clowe, D.; et al. Direct Constraints on the Dark Matter Self-Interaction Cross Section from the Merging Galaxy Cluster 1E 0657-56. *Astrophys. J.* **2004**, *606*, 819.